Int J Thermophys (2009) 30:1864–1874
DOI 10.1007/s10765-009-0666-3

Measurement of the Thermal Conductivity of Nanodeposited Material

Koji Takahashi · Norsyazwan Hilmi · Yohei Ito · Tatsuya Ikuta · Xing Zhang

Received: 30 January 2009 / Accepted: 15 October 2009 / Published online: 4 November 2009
© Springer Science+Business Media, LLC 2009

Abstract The small size of nanomaterials deposited by either focused ions or electron beams has prevented the determination of reliable thermal property data by existing methods. A new method is described that uses a suspended platinum hot film to measure the thermal conductivity of a nanoscale deposition. The cross section of the Pt film needs to be as small as 50 nm × 500 nm to have sufficient sensitivity to detect the effect of the beam-induced nanodeposition. A direct current heating method is used before and after the deposition, and the change in the average temperature increase of the Pt hot film gives the thermal conductivity of the additional deposited material. In order to estimate the error introduced by the one-dimensional analytical model employed, a two-dimensional numerical simulation was conducted. It confirmed the reliability of this method for situations where the deposit extends onto the terminals by 1 μm or more. Measurements of amorphous carbon (a-C) films fabricated by electron beam induced deposition (EBID) produced thermal conductivities of $0.61\ \mathrm{W \cdot m^{-1} \cdot K^{-1}}$ to $0.73\ \mathrm{W \cdot m^{-1} \cdot K^{-1}}$ at 100 K to 340 K, values in good agreement with those of a-C thin films reported in the past.

Keywords Electron beam induced deposition · Nano sensor · Thermal conductivity · Thin film

K. Takahashi (✉) · N. Hilmi · Y. Ito · T. Ikuta
Graduate School of Engineering, Kyushu University, Fukuoka 819-0395, Japan
e-mail: takahashi@aero.kyushu-u.ac.jp

X. Zhang
Department of Engineering Mechanics, Tsinghua University, 100084 Beijing, China

1 Introduction

There has been rapid progress in the synthesis and processing of nanoscale materials such as nanotubes, nanowires, and thin films. As the application area of these materials widen, a knowledge of their thermal properties is recognized as an important issue. However, measuring the thermal properties of nanostructures remains a challenging task. The major problems are experimental difficulties in determining accurate thermal property values [1,2] due to the limited capabilities for handling such increasingly downsized specimens. Recent studies have revealed that the thermal conductivities of nanoscale materials are different from those of their corresponding bulk materials due to the boundary scattering effect of phonons, as well as the intrinsic atomic-level structural differences. In order to explore this new thermophysical target, it is vital to develop special instrumental methods that match the size and shape of these nanoscale materials.

So far, measurement techniques for thermal properties of large area thin films have been extensively studied for the purpose of the thermal management of electronic devices. However, such methods cannot be applied to specimens whose overall size is less than 1 μm. For example, thermoreflectance gives accurate data but its best spatial resolution is still greater than 3 μm [3]. Scanning thermal microscopy has distinguished spatial features smaller than 100 nm but a reliable property measurement is still missing because of the complex tip-sample conduction mechanisms, coupled with the effect of surface topography. On the other hand, a strong demand for measuring the thermal conductivity of carbon nanotubes inspired researchers to invent a new nanoscale thermal sensor [4]; this sensor was successfully applied to other nanowires [5]. However, the recently realized three-dimensional nanostructures still lack thermal property data. These nanostructures are made by an accumulation of extremely tiny amounts of deposits, called nanodeposition, built by either focused ion beam (FIB) [6] or electron-beam-induced deposition (EBID) methods [7,8]. Because the physical property of such a nanodeposition is expected to depend not only on its size, but also on the process conditions, it is desirable to develop a new reliable measurement method for such nanoscale regime depositions.

Here we report on an in-plane thermal-conductivity measurement of nanodeposition employing a suspended platinum (Pt) nanofilm that is as small as the beam-induced deposition. The most important characteristic of our device is the use of a suspended nanofilm as the sensor, having the advantages of simplicity as well as high accuracy. In this work, we examine an amorphous carbon (a-C) film deposited by EBID. This nanofabrication technique uses a high intensity electron beam to directly deposit solid nanostructures on a substrate surface as a result of secondary-electron-induced dissociation of precursor molecules absorbed on the surface [9]. Recently, there has been much interest in the applications of EBID a-C nanostructures, not only for adhesive coatings [10], but for practical electronic devices [11], because EBID can be carried out with no special equipment other than a scanning electron microscope (SEM).

However, it is well known that carbon thin films can exhibit a variety of thermal property values [12,13], depending on the fractions of sp^2 and sp^3 bonds, hydrogen content, density, etc. Such data are difficult to obtain for EBID nanostructures due to their small size—for example, the Raman spectrum of a very small a-C deposit is too

noisy to allow this method to characterize its microstructure. Overall, there is still a limited understanding of the thermal properties of a-C films despite numerous studies reported on their fabrication techniques and possible applications. Our approach is not to extrapolate the thermal property from other chemical or structural information, but to directly measure the property of the nanodeposited material itself.

2 Principle of Measurement

We use a Pt nanofilm as employed in the previously reported device [4], a study in which the thermal properties of individual carbon nanotubes were measured. The suspended nanofilm serves as a heater that provides uniform heat generation and acts as an electrical thermometer. All measurements are conducted in a 1.0×10^{-3} Pa vacuum environment, and the nanofilm undergoes a temperature increase of about 10 K. The residual gas heat conduction in this pressure range and thermal radiation losses calculated from the Stefan–Boltzmann law can be neglected. Hence, for the case of a constant heating current, the heat transfer along this nanofilm can be treated by a one-dimensional steady-state heat conduction model [14] of the sort shown in Fig. 1a. The temperature distribution along the nanofilm, $T(x)$, is given by

$$T(x) = T_0 + \frac{IV}{2wd\lambda}x - \frac{IV}{2lwd\lambda}x^2 \tag{1}$$

where x is the distance between the connection of the nanofilm and the terminal which serves as a heat sink kept at temperature T_0 during the measurement, I is the applied heating current, V is the voltage, l is the nanofilm length, w is its width, d is its thickness, and λ is the thermal conductivity. Furthermore, the average temperature increase along the nanofilm, ΔT_L, can be calculated from Eq. 1 and the mean temperature of the nanofilm can be determined from the following equation:

$$\overline{T} = T_0 + \Delta T_L = T_0 + \frac{IV}{\lambda}\frac{l}{12wd} \tag{2}$$

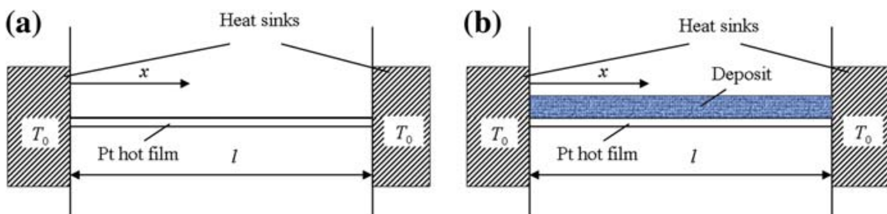

Fig. 1 Thermal measurement model using a Pt hot film suspended between two terminals at constant temperature. The thermal conductivity of the deposited material is obtained by the thermal conductance change between just (**a**) the Pt film and (**b**) the Pt film covered with a deposit

The thermal conductivity of the nanofilm is then obtained through the following equation:

$$\lambda = \frac{l}{12wd}\frac{IV}{\Delta T_L} \quad (3)$$

The mean temperature of the nanofilm is also associated with the electrical and the temperature coefficient of resistance (TCR) by

$$\overline{T} = T_s + \frac{R - R_s}{\beta R_s} \quad (4)$$

where $T_s = 273.2$ K is the reference temperature and R_s is the reference resistance of the Pt nanofilm at 273.2 K, R is the nanofilm resistance, and β is the TCR of the nanofilm. Combining Eqs. 2 and 4, the resistance of the nanofilm R is obtained as

$$R = R_0 + \frac{\beta R_s}{\lambda}\frac{l}{12wd}IV \quad (5)$$

where R_0 is the resistance at temperature T_0, which can be determined by extrapolating the heating power to zero.

To measure the thermal conductivity of a nanodeposit, the principle proposed here is to deposit the material onto a suspended Pt nanofilm as shown in Fig. 1b. Thus, the thermal conductivity of the nanostructure can be estimated by comparing the thermal conductance $G = \lambda wd/l$ obtained from Eq. 5 for the Pt nanofilm alone and for the Pt nanofilm with the nanodeposit. Based on the assumption that the electrical conductivity of Pt is several orders larger than that of a-C, when a heating current is applied to the lead, Joule heating will occur only in the Pt nanofilm. A certain amount of generated heat will be absorbed by the deposit; both the heat from the Pt nanofilm and that from the a-C are then transferred to the heat sink situated at each end of the film. By considering the thermal circuit of the present experimental arrangement, the thermal conductance found from the second measurement can be roughly expressed as $G_{\text{a-C/Pt}} = G_{\text{pt}} + G_{\text{a-C}}$, where G_{pt} is that obtained from the first measurement before deposition. Then, the thermal conductivity of the nanodeposited material is calculated from its observed size.

Since, in some cases, employing a one-dimensional heat transfer approach oversimplifies the problem, further investigations of the thermal transport using a numerical simulation helped us to fully comprehend its behavior in the current system. Although a one-dimensional model is sufficient for estimating the thermal conductivity of a Pt nanofilm [15], in the case of a Pt nanofilm with a thick a-C deposit, there might be two-dimensional heat transfer taking place within the a-C layer, because a-C is known to have a low thermal conductivity.

Therefore, we compared the results of one- and two-dimensional calculations to account for the two-dimensional effects. The numerical calculation employed is based on the finite-different method using 10 nm × 10 nm grids. The model for two-dimensional numerical heat transfer analysis is shown in Fig. 2, where we treat one-half of a 10 μm long film, with the a-C over-deposited on the terminal by 1 μm. The reason

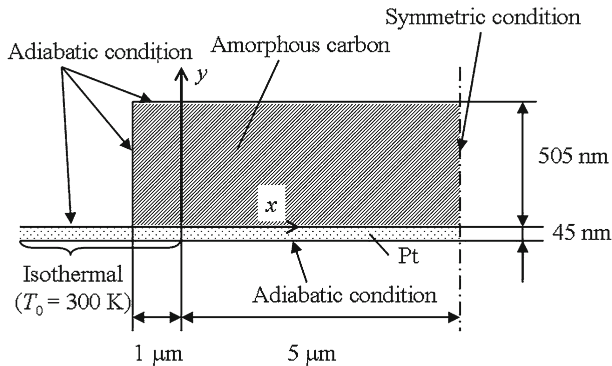

Fig. 2 Calculation model and boundary conditions for the two-dimensional heat transfer numerical simulation, for the case where the deposit over-coats the heat-sink terminal to a length of 1 μm

for this over-deposition is explained later. The thermal conductivities of Pt and a-C are set at $30.0\,\mathrm{W \cdot m^{-1} \cdot K^{-1}}$ and $1.0\,\mathrm{W \cdot m^{-1} \cdot K^{-1}}$, respectively. The calculated temperature distributions in the a-C layer along the y-direction shown in Fig. 3a are almost flat curves. These results are essentially identical to those from the one-dimensional model; the comparison of the one- and two-dimensional heat transfer calculations in Fig. 3b shows that the difference in the mean temperature increase is just 3.1 %. Because the resulting error for thermal-conductivity measurements due to the one-dimensional assumption is the same as this temperature difference, we can conclude that this error is negligible compared with other experimental uncertainties represented by the size measurement of the a-C deposit. Basically, a thicker deposition of lower thermal conductivity induces a larger deviation from the one-dimensional model. The quantitative discussion on this kind of error needs numerical calculation but is not conducted here. There is another limitation of the current method, in that we cannot measure deposits smaller than the Pt sensor. The smallest surface of our fabricated Pt hot-film is approximately 2 μm × 100 nm. However, because the beam-scanning technique can easily enlarge the deposition size, we can estimate the thermal conductivity of almost all kinds of beam-induced nanodeposits.

In addition, two other calculations for different over-deposition lengths of 0 μm and 2 μm were conducted. The obtained errors were 5.5 % and 3.1 %, respectively. The larger error for no over-deposition of the a-C film on the lead is probably due to the one-dimensional analysis neglecting the two-dimensional heat flow around the adiabatic edge. However, an over-deposition of 1 μm thickness is sufficient to reduce this effect. Based on these numerical results, we conducted thermal-conductivity measurements for nanodeposits which were over-deposited by at least 1 μm on the terminal when using a 5 μm long Pt film.

3 Experimental

A schematic diagram of the experimental apparatus and the measuring circuit are shown in Fig. 4. For all measurements, the substrate is mounted on the sample holder

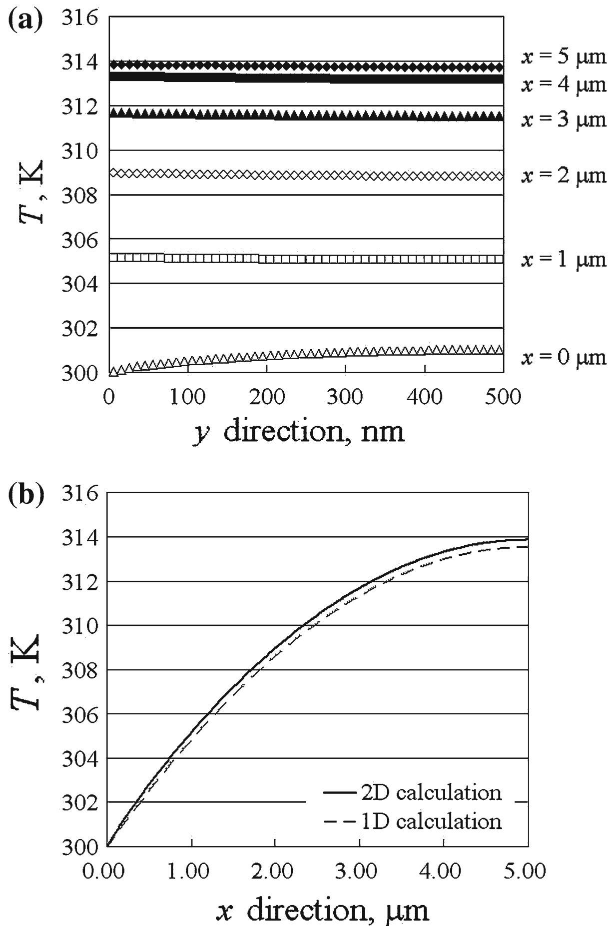

Fig. 3 Results of two-dimensional heat transfer simulation: (**a**) temperature distributions in the deposit along the y direction and (**b**) comparison of temperature profiles of Pt film using one-dimensional and two-dimensional models; two-dimensional model predictions are 3.1 % higher

of a liquid-nitrogen cryostat (Oxford Instruments, Optistat DN-V). The measurement chamber is continuously evacuated using a molecular pump. The temperature of the sample holder can be controlled from 77 K to 500 K using a PID temperature controller. The measurement system consists of a high accuracy power supply (Advantest R6243), two high accuracy digital multimeters (Keithley 2002, 8.5 digits), a standard resistance (Yokogawa 2792), and the sample. Figure 5a shows the Pt nanofilm prepared for the current experiment, fabricated using electron beam lithography and MEMS techniques as described previously [15]. A Si substrate with a 180 nm thick SiO_2 layer is used as the starting material. An EB resist of 320 nm in thickness is spin-coated on the substrate, and the electron-beam lithography system is used to directly draw the nanofilm and terminal leads on the EB resist. A 5 nm thick titanium adhesion layer and a 40 nm thick platinum film are then deposited by electron-beam physical

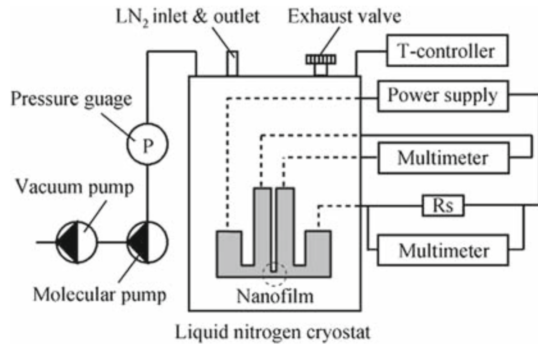

Fig. 4 Schematic diagram of the experimental apparatus and measuring circuit

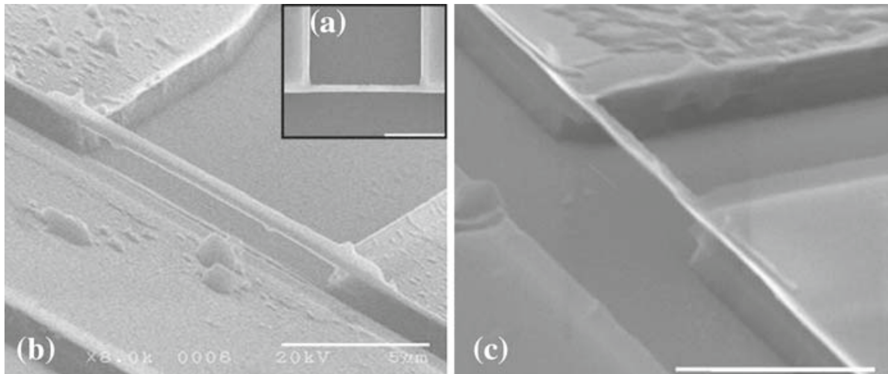

Fig. 5 SEM images of Pt films: (**a**) Pt nanofilm prepared for the measurement, (**b**) tilted images of Pt nanofilm after a-C deposition, and (**c**) Pt film after a-C removal. *White scale bars* are 5 µm

vapor deposition, and the exact film thickness is measured afterwards using an atomic force microscope (AFM). To make a suspended Pt nanofilm, a lift-off technique is used where the substrate is immersed in a liquid resist-remover to leave only the Pt/Ti pattern on the SiO_2 layer. Then, isotropic etching using buffered hydrofluoric acid is employed to remove the SiO_2 and titanium layer around the nanofilm. Finally, the Si substrate is slightly etched using a KOH solution to completely detach the nanofilm from the substrate. The fabricated device shown in Fig. 5 consists of a suspended nanofilm 9.34 µm in length, with a width of 509 nm and a thickness of 44 nm, connected to terminal leads.

First, we measured the intrinsic electrical and thermal properties of the Pt nanofilm. Figure 6 shows the dependence of the measured electrical resistance R on the heating power IV. The linearity of the results in Fig. 6a suggests the validity of one-dimensional analysis expressed in Eq. 5. The thermal conductivity calculated from this curve is discussed later. The electrical resistivity $\rho = wdR/l$ of the nanofilm is compared with that of bulk platinum in Fig. 6b. Because the electron mean free path is reduced by electron scattering at the film and grain boundaries, the conductivity varies for each film, which means this measurement is needed for each sensor.

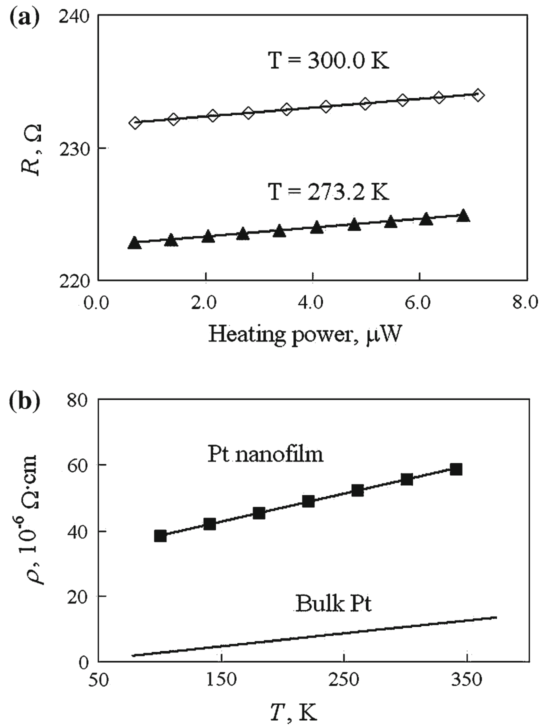

Fig. 6 Measured electrical properties of fabricated Pt film: (**a**) dependence of the resistance on the heating power; data extrapolated to zero heating power are the intrinsic electrical resistances at each temperature and (**b**) electrical resistivity of the fabricated Pt nanofilm compared with that of bulk Pt material for temperatures from 100 K to 340 K

After its intrinsic properties have been measured, the Pt nanofilm is transferred to a S-4300SE (Hitachi) SEM for the a-C EBID procedure. The conditions were a 5 kV accelerating voltage and 100 pA electron beam current using *n*-tetracosane ($C_{24}H_{50}$) as the paraffin precursor as described by Ding et al. [9]. The a-C is deposited by positioning and scanning the electron beam on the Pt nanofilm using the SEM line-scanning mode exposed for about 40 min. Figure 5b shows that the a-C nanodeposit is fabricated uniformly onto the Pt nanofilm with a thickness of 563 nm and a width of 749 nm. Round and dot-shaped deposits were also observed around the target area. These are fragments of the precursor or secondary deposits [16] due to electrons laterally scattered from the deposited a-C on the Pt nanofilm. These unexpected deposits formed on the substrates and terminals do not affect the measurement. After the EBID procedure is completed, the device is transferred into the cryostat for the second measurement to determine the thermal conductivity as quickly as possible because the oxidation of a-C occurs in air even at room temperature and can reduce the volume of the nanodeposit significantly.

There is a critical issue affecting the measurement accuracy that has to be considered very carefully, which is the effect of the electron beam used during EBID on the characteristics of the Pt nanofilm. In order to verify that the electron beam irradiation during the EBID procedure is not changing the properties of the Pt film, another experiment was carried out that totally removed the a-C nanodeposit from the Pt nanofilm using an oxygen plasma. This a-C removal procedure was conducted in

a PR500 Yamato plasma reactor using $60\,\mathrm{mL} \cdot \mathrm{min}^{-1}$ oxygen gas flow and a power level of 150 W at 13.56 MHz for 5 min, repeated five times at intervals of 2 min in order to avoid an unnecessary temperature rise that might affect the microstructure of the nanofilm.

Figure 5c shows a SEM picture of the Pt nanofilm after the a-C removal procedure. This nanofilm is measured again to investigate any change in the electrical properties due to the annealing process occurring during both electron-beam irradiation and oxygen plasma processes. We confirmed that the electrical conductivities of the initial measurement and after a-C removal differ by only 1 % to 2 % over the entire temperature range. This means that the electron beam irradiation during the EBID procedure does not affect the Pt nanofilm. We do not intend to focus on the reasons in this paper, but our results suggest that the electron beam has a low enough energy to avoid causing any damage, nor significantly changing the Pt nanofilm characteristic. The a-C layer deposited on the Pt nanofilm may act as a protective coating to prevent the electron beam from damaging the Pt nanofilm. The interaction of EBID processing and the suspended film has to be explored and understood in the future, as suggested in the review of Randolph et al. [17]. Considering that the slight change observed of 1 % to 2 % is possibly due simply to the connections error between the Pt leads and measurement instruments, which can be improved by taking proper precautions, it can be concluded that this new method provides a reliable means to obtain the thermal conductivity of the a-C nanodeposit.

4 Results and Discussion

Figure 7 shows the measured thermal conductance of the initial Pt nanofilm and after a-C nanodeposition. For temperatures from 100 K to 340 K, the calculated thermal conductivities of the Pt nanofilm range between $23.0\,\mathrm{W \cdot m^{-1} \cdot K^{-1}}$ and $37.0\,\mathrm{W \cdot m^{-1} \cdot K^{-1}}$, values which are much lower than that of bulk Pt, but consistent with those in a previous report [15]. The Pt nanofilm covered with a-C shows a similar temperature dependence as the clean Pt film, but exhibits only about a

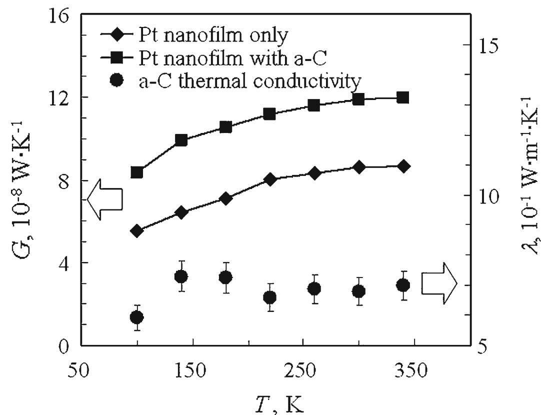

Fig. 7 Measured thermal conductances of a Pt nanofilm, and of a Pt nanofilm after deposition of a-C. This result shows 40 % to 50 % increase in the conductance due to the a-C nanodeposit. Calculated thermal conductivities of a-C nanodeposition are shown by the *solid circles* with error bars

40 % to 50 % increase in the thermal conductance value, suggesting that this additional thermal conductance is definitely due to the heat transferred through the a-C layer. Making this assumption, comparing the two conductances affords an estimate of the thermal conductivity of the additional a-C layer ranging from $0.61\,\mathrm{W \cdot m^{-1} \cdot K^{-1}}$ to $0.73\,\mathrm{W \cdot m^{-1} \cdot K^{-1}}$ for temperatures between 100 K and 340 K, as shown by the solid circles in Fig. 7. This result is in good agreement with past reports [12,13] for large area thin films. Furthermore, it is physically consistent with the thermal-conductivity characteristics of amorphous materials, which have no peak and slightly increases with temperature because phonon–phonon umklapp scattering does not dominate the boundary scattering in this temperature range.

The effect of the thermal contact resistance at the a-C/Pt interface regions is the last issue to be considered. There are no measured data of the contact resistance for a-C/Pt, but its effect can be estimated from the data for Si/SiO_2, which was measured by Yamane et al. [18] as $1.0 \times 10^{-8}\,\mathrm{m^2 \cdot K \cdot W}$. Because contamination at the a-C/Pt interface region is removed during the EBID procedure and no voids were found at the interface in our TEM observations, the contact resistance is not likely to be much larger than that of Ref. [18]. We reworked the numerical simulation using this contact resistance and found that the thermal conductivity of an a-C layer increased by 3.9 %. This error is negligible compared with other experimental uncertainties. Although further investigation of the contact problem and more detailed investigation of the measurement errors are required, we have shown that this method is reliable enough to conduct thermal-conductivity measurements of locally deposited nanostructures.

5 Concluding Remarks

We have shown that a suspended Pt nanofilm can be used to obtain the in-plane thermal conductivity of a nanodeposit. The measurement method is formulated on the basis of one-dimensional heat transfer analysis, but consideration of two-dimensional heat flow and contact resistance show the reliability of this method. We have demonstrated the viability of this technique using EBID a-C, but it is applicable to deposited material of any type—insulators, semiconductors, and even conductors—simply by coating the Pt nanofilm with the appropriate material. Because there is no upper limit of the deposited area, not only these nanodeposits but normal thin films fabricated by sputtering or physical/chemical vapor deposition methods can be measured. Then, their local thermal conductivity can be obtained with micrometer-order resolution in the same manner. As there is currently no reliable measurement method for the in-plane thermal conductivity of nanoscale deposits or that of micrometer-order resolution, the technique reported here should play an important role in solving the continuing challenges of micro- and nanoscale engineering.

Acknowledgments This work was partially supported by a Grant in Aid for Scientific Research (20360099, 20656140, 20048006). The authors thank Prof. Motoo Fujii for valuable advice on measurement techniques, and part of the sensor fabrication was conducted at the Collabo-station II, Kyushu University.

References

1. D.G. Cahill, K.E. Goodson, A. Majumdar, J. Heat Transfer **124**, 223 (2002)
2. D.G. Cahill, W.K. Ford, K.E. Goodson, G.D. Mahan, A. Majumdar, H.J. Maris, R. Merlin, S.R. Phillpot, J. Appl. Phys. **93**, 793 (2003)
3. S. Huxtable, D.G. Cahill, V. Fauconnier, J.O. White, J.-C. Zhao, Nat. Mater. **3**, 298 (2004)
4. M. Fujii, X. Zhang, H. Xie, H. Ago, K. Takahashi, T. Ikuta, H. Abe, T. Shimizu, Phys. Rev. Lett. **5**, 065502 (2005)
5. K. Takahashi, Y. Ito, T. Ikuta, T. Nishiyama, M. Fujii, X. Zhang, A. Huczko, High Temp.–High Press. **37**, 119 (2008)
6. S. Matsui, T. Kaito, J. Fujita, M. Komuro, K. Kanda, Y. Haruyama, J. Vac. Sci. Tech. **18**, 3181 (2000)
7. N. Silvis-Cividjian, C.W. Hagen, P. Kruit, M.A.J.v.d. Stam , H.B. Groen, Appl. Phys. Lett. **82**, 20 (2003)
8. T. Bret, I. Utke, P. Hoffmann, Microelectron. Eng. **78–79**, 307 (2005)
9. W. Ding, D.A. Dikin, X. Chen, R.D. Piner, X. Wang, X. Li, R.S. Ruoff, E. Zussman, J. Appl. Phys. **98**, 014905 (2005)
10. H. Nishijima, S. Kamo, S. Akita, Y. Nakayama, K.I. Hohmura, S.H. Yoshimura, K. Takeyasu, Appl. Phys. Lett. **74**, 4061 (1999)
11. S.R.P. Silva, J.D. Carey, Diam. Relat. Mater. **12**, 151 (2003)
12. A.J. Bullen, K.E. O’Hara, D.G. Cahill, O. Monteiro, A. von Keudell, J. Appl. Phys. **88**, 6317 (2000)
13. M. Shamsa, W.L. Liu, A.A. Balandin, C. Casiraghi, W.I. Milne, A.C. Ferrari, Appl. Phys. Lett. **89**, 161921 (2006)
14. Q.C. Zhang, B.Y. Cao, X. Zhang, M. Fujii, K. Takahashi, J. Phys. Condens. Matter **18**, 7937 (2006)
15. X. Zhang, H. Xie, M. Fujii, K. Takahashi, T. Ikuta, H. Ago, H. Abe, T. Shimizu, Int. J. Heat Mass Transfer **49**, 3879 (2006)
16. T. Bret, I. Utke, P. Hoffmann, M. Abourida, P. Doppelt, Microelectron. Eng. **83**, 1482 (2006)
17. S.J. Randolph, J.D. Fowlkes, P.D. Rack, J. Appl. Phys. **97**, 124312 (2005)
18. T. Yamane, N. Nagai, S. Katayama, M. Todoki, J. Appl. Phys. **91**, 9772 (2002)